arXiv:1212.1283v1 [cs.IT] 6 Dec 2012

A Tractable Framework for Exact Probability of Node Isolation in Finite Wireless Sensor Networks

Salman Durrani, *Senior Member, IEEE*, Zubair Khalid, *Student Member, IEEE* and Jing Guo

Abstract

This paper presents a tractable analytical framework for the exact calculation of probability of node isolation when N sensor nodes are independently and uniformly distributed inside a finite square region. The proposed framework can accurately account for the boundary effects by partitioning the square into subregions, based on the transmission range and the node location. We show that for each subregion, the probability that a random node falls inside a disk centered at an arbitrary node located in that subregion can be expressed analytically in closed-form. Using the results for the different subregions, we obtain the exact probability of node isolation and an upper bound for the probability of connectivity. The proposed framework is validated by comparison with simulation results and provides a very powerful tool to accurately account for the boundary effects in finite wireless sensor networks.

Index Terms

Wireless sensor networks, probability of node isolation, probability of connectivity, boundary effects.

The authors are with the Research School of Engineering, College of Engineering and Computer Science, The Australian National University, Canberra, ACT 0200, Australia. Emails: {salman.durrani, zubair.khalid, jing.guo}@anu.edu.au

I. INTRODUCTION

Connectivity is a basic requirement for the planning and effective operation of wireless sensor networks [1], [2]. The probability of the network being connected (referred to as probability of connectivity) is defined as the probability that every node pair in the network has at least one path connecting them. The probability of node isolation, which is defined as the probability that a randomly selected node has no connections to any other nodes, plays a key role in determining the overall network connectivity [3], [4]. When the node locations follow an infinite homogeneous Poisson point process and assuming all nodes have the same transmission range, it has been shown that the probability of connectivity becomes 1 at the same time as when there are no isolated nodes [5]. For large-scale wireless sensor networks, assuming Poisson distributed nodes in an infinite area, the connectivity behaviour in terms of probability of node isolation or the probability of connectivity has been well studied [3], [5]–[8].

Recently there has been an increasing interest to model the connectivity properties in finite wireless sensor networks [4], [9]–[13]. This is because many practical wireless sensor networks are formed by distributing a finite (small) number of nodes in a finite area, which is typically assumed to be a square region [14], [15]. It has been shown that the asymptotic connectivity results for large-scale wireless sensor networks provide an extremely poor approximation for finite wireless sensor networks [11]. This is due to the boundary effects, i.e., the nodes located close to the physical boundaries of the network have a limited coverage area and hence greater probability of isolation. The boundary effects play an important role in determining the overall network connectivity properties.

Different approaches have been used in the literature, to try to model the boundary effects including (i) using geometrical probability [16] and dividing the square into smaller squares to facilitate asymptotic analysis [9], (ii) using a cluster expansion approach and decomposing the boundary effects into corners and edges to yield high density approximations [13] and (iii) using a deterministic grid deployment of nodes in a finite area [17] to approximate the boundary effects with random deployment of nodes [11]. The above approaches provide bounds, rather than exact results, for the probability of node isolation and/or probability of connectivity. To the best of our knowledge, the exact probability of node isolation when N nodes are independently and uniformly distributed inside a finite square region is not available in the literature.

In this correspondence, we present a tractable analytical framework for the exact calculation of the probability of node isolation in finite wireless sensor networks, when N nodes are independently and uniformly distributed in a square region. The proposed framework is based on partitioning the square into unequal subregions, based on the transmission range and the location of an arbitrary node. Using geometrical probability, we show that for each subregion, the probability that a random node falls inside a disk centered at an arbitrary node located in that subregion can be expressed analytically in closed-form. This framework accurately models the boundary effects and leads to an exact expression for the probability of node isolation and an upper bound for the probability of connectivity, which can be easily evaluated numerically. The analysis is validated by comparison with simulations as well as existing results.

The following notations will be used in the correspondence: $(x,\, y)$ denotes the coordinates of a point, $\mathrm{abs}(\cdot)$ denotes the absolute value or modulus and $|\mathcal{R}|$ denotes the area of the two dimensional region $\mathcal{R}$.

II. SYSTEM MODEL

Consider N nodes which are uniformly and independently distributed inside a square region $\mathcal{R} \in \mathbb{R}^2$, where $\mathbb{R}^2$ denotes the two dimensional Euclidean domain. Let S_ℓ and V_ℓ, for $\ell \in \{1, 2, 3, 4\}$, denote the side and vertex of the square, respectively, which are numbered in an anticlockwise direction. Without loss of generality, we assume that the first vertex V_1 of the square is located at the origin $(0, 0)$ and we consider a unit square region defined as

$$\mathcal{R} = \{\boldsymbol{u} = (x, y) \in \mathbb{R}^2 |\, 0 \le x \le 1,\, 0 \le y \le 1\}. \tag{1}$$

Let $\boldsymbol{u} = (x, y)$ denote the position of an arbitrary node inside the square $\mathcal{R}$. The node distribution probability density function (PDF) can be expressed as

$$f_{\mathrm{U}}(\boldsymbol{u}) = \begin{cases} 1 & \boldsymbol{u} \in \mathcal{R}, \\ 0 & \boldsymbol{u} \in \mathbb{R}^2 \backslash \mathcal{R}. \end{cases} \tag{2}$$

We define $|\mathcal{R}| = \int_{\mathcal{R}} ds(\boldsymbol{u})$ as a measure of the physical area of the square region, where $ds(\boldsymbol{u}) = dxdy$. Note that $|\mathcal{R}| = 1$ since we have assumed a unit square.

Our main objective is to obtain an exact expression for the probability of node isolation, which is tractable. Assuming each sensor node has a fixed transmission range r_{o}, the coverage region of each node will be a disk $\mathcal{D}(\boldsymbol{u}; r_{\text{o}})$ of radius r_{o} centered at the node. Note that $|\mathcal{D}(\boldsymbol{u}; r_{\text{o}})| = \pi r_{\text{o}}^2$. An arbitrary node will be isolated if there is no node located inside $\mathcal{D}(\boldsymbol{u}; r_{\text{o}})$. Let the cumulative density function (CDF) $F(\boldsymbol{u}; r_{\text{o}})$ denote the probability that a random node falls inside the disk $\mathcal{D}(\boldsymbol{u}; r_{\text{o}})$ of radius r_{o} centered at $\boldsymbol{u}$. Following [18], this probability can be calculated using the overlap area between the disk $\mathcal{D}(\boldsymbol{u}; r_{\text{o}})$ and square $\mathcal{R}$ as

$$F(\boldsymbol{u}; r_{\text{o}}) \;=\; \frac{|\mathcal{D}(\boldsymbol{u}; r_{\text{o}}) \cap \mathcal{R}|}{|\mathcal{R}|}. \tag{3}$$

Assuming that the probability of node isolation is independent for each node, the conditional probability of node isolation (conditioned on knowing the location of the arbitrary node) can be expressed as

$$P_{\text{iso}}(\boldsymbol{u}; r_{\text{o}}) \;=\; \left(1 - F(\boldsymbol{u}; r_{\text{o}})\right)^{N-1}. \tag{4}$$

The probability of node isolation can be calculated by weighting with $f_{\mathbf{U}}(\boldsymbol{u})$ and averaging over all possible locations of the arbitrary node $\boldsymbol{u} \in \mathcal{R}$ as

$$P_{\text{iso}}(r_{\text{o}}) \;=\; \int_{\mathcal{R}} P_{\text{iso}}(\boldsymbol{u}; r_{\text{o}}) f_{\mathbf{U}}(\boldsymbol{u}) ds(\boldsymbol{u}). \tag{5}$$

Using (4), we can find the probability of no isolated node, which can be used to obtain an upper bound for the probability of overall network connectivity as [4]

$$P_{\text{con}}(r_{\text{o}}) \leq P_{\text{no-iso}}(r_{\text{o}}) \;=\; \left(1 - P_{\text{iso}}(r_{\text{o}})\right)^{N}. \tag{6}$$

Note that it is also possible to use a first order linear approximation and express (6) as $P_{\text{con}}(r_{\text{o}}) \leq P_{\text{no-iso}}(r_{\text{o}}) \;\approx\; 1 - N P_{\text{iso}}(r_{\text{o}})$ [11]. However, we will use (6) directly in this paper.

III. PROBLEM FORMULATION

There are two key challenges in evaluating (3)−(6). The *first challenge* is to find the CDF in (3), which requires the evaluation of the overlap area $|\mathcal{D}(\boldsymbol{u}; r_{\rm o}) \cap \mathcal{R}|$. In [10], it is proposed to find this intersection area using polar coordinates and dividing the square into different radial regions. However, due to the dependance between the polar radius and the polar angle, this approach does not lead to closed-form solutions. In [18], an alternative approach is presented for finding the intersection area by first finding the area of circular segments formed outside the sides and vertices and then subtracting from the area of the disk. This approach leads to closed-form solutions and is adopted in this work. The basic building blocks in this approach to characterise the *boundary effects* are (i) the circular segment areas formed outside each side (*border effects*) and (ii) the corner overlap areas between two circular segments formed at each vertex (*corner effects*).

Let $B_1(\boldsymbol{u}; r_{\rm o})$ denote the area of the circular segment formed outside the side S_1, as illustrated in Fig. 1. Using the fact that the area of the circular segment is equal to the area of the circular sector minus the area of the triangular portion, we obtain

$$B_1(\boldsymbol{u}; r_{\rm o}) = r_{\rm o}^2 \arccos\left(\frac{x}{r_{\rm o}}\right) - x\sqrt{r_{\rm o}^2 - x^2}. \tag{7}$$

Similarly, the areas of the circular segments formed outside the sides S_2, S_3 and S_4, respectively, can be expressed as

$$B_2(\boldsymbol{u}; r_{\rm o}) = r_{\rm o}^2 \arccos\left(\frac{y}{r_{\rm o}}\right) - y\sqrt{r_{\rm o}^2 - y^2}, \tag{8}$$

$$B_3(\boldsymbol{u}; r_{\rm o}) = r_{\rm o}^2 \arccos\left(\frac{1-x}{r_{\rm o}}\right) - (1-x)\sqrt{r_{\rm o}^2 - (1-x)^2}, \tag{9}$$

$$B_4(\boldsymbol{u}; r_{\rm o}) = r_{\rm o}^2 \arccos\left(\frac{1-y}{r_{\rm o}}\right) - (1-y)\sqrt{r_{\rm o}^2 - (1-y)^2}. \tag{10}$$

Let $C_1(\boldsymbol{u}; r_{\rm o})$ denote the area of the corner overlap region between two circular segments at vertex V_1, as illustrated in Fig. 1. Using the fact that the area of the overlap region is equal to the area of the circular sector minus the area of two triangular portions, we can easily show that

$$C_1(\boldsymbol{u}; r_{\rm o}) = \frac{1}{2} r_{\rm o}^2 \theta - \frac{1}{2}\left(\sqrt{r_{\rm o}^2 - y^2} - x\right) y - \frac{1}{2}\left(\sqrt{r_{\rm o}^2 - x^2} - y\right) x, \tag{11}$$

where the angle θ is given by

$$\theta \,=\, 2\arcsin\left(\frac{\mathrm{abs}\left(\sqrt{\theta_1}\,\right)}{2r_{\mathrm{o}}}\right), \tag{12}$$

where $\theta_1 = 2r_{\mathrm{o}}^2 - 2x\sqrt{r_{\mathrm{o}}^2 - y^2} - 2y\sqrt{r_{\mathrm{o}}^2 - x^2}$. Similarly, the areas of the corner overlap region formed at vertex V_2, V_3 and V_4, respectively, can be expressed as

$$C_2(\boldsymbol{u}; r_{\mathrm{o}}) \,=\, \frac{1}{2}r_{\mathrm{o}}^2\alpha - \frac{1}{2}\left(\sqrt{r_{\mathrm{o}}^2 - y^2} - (1-x)\right)y - \frac{1}{2}\left(\sqrt{r_{\mathrm{o}}^2 - (1-x)^2} - y\right)(1-x), \tag{13}$$

$$C_3(\boldsymbol{u}; r_{\mathrm{o}}) \,=\, \frac{1}{2}r_{\mathrm{o}}^2\beta - \frac{1}{2}\left(\sqrt{r_{\mathrm{o}}^2 - (1-y)^2} - (1-x)\right)(1-y) - \frac{1}{2}\left(\sqrt{r_{\mathrm{o}}^2 - (1-x)^2} - (1-y)\right)(1-x), \tag{14}$$

$$C_4(\boldsymbol{u}; r_{\mathrm{o}}) \,=\, \frac{1}{2}r_{\mathrm{o}}^2\gamma - \frac{1}{2}\left(\sqrt{r_{\mathrm{o}}^2 - (1-y)^2} - x\right)(1-y) - \frac{1}{2}\left(\sqrt{r_{\mathrm{o}}^2 - x^2} - (1-y)\right)x, \tag{15}$$

where the angles α, β and γ are given by

$$\alpha \,=\, 2\arcsin\left(\frac{\mathrm{abs}\left(\sqrt{\alpha_1}\right)}{2r_{\mathrm{o}}}\right) \tag{16}$$

$$\beta \,=\, 2\arcsin\left(\frac{\mathrm{abs}\left(\sqrt{\beta_1}\right)}{2r_{\mathrm{o}}}\right) \tag{17}$$

$$\gamma \,=\, 2\arcsin\left(\frac{\mathrm{abs}\left(\sqrt{\gamma_1}\right)}{2r_{\mathrm{o}}}\right) \tag{18}$$

where $\alpha_1 = 2r_{\mathrm{o}}^2 - 2(1-x)\sqrt{r_{\mathrm{o}}^2 - y^2} - 2y\sqrt{r_{\mathrm{o}}^2 - (1-x)^2}$, $\beta_1 = 2r_{\mathrm{o}}^2 - 2(1-x)\sqrt{r_{\mathrm{o}}^2 - (1-y)^2} - 2(1-y)\sqrt{r_{\mathrm{o}}^2 - (1-x)^2}$ and $\gamma_1 = 2r_{\mathrm{o}}^2 - 2x\sqrt{r_{\mathrm{o}}^2 - (1-y)^2} - 2(1-y)\sqrt{r_{\mathrm{o}}^2 - x^2}$.

Using (7)$-$(10) and (11), (13)$-$(15), the CDF $F(\boldsymbol{u}; r_{\mathrm{o}})$ in (3) can be expressed in closed-form, e.g., if $r_{\mathrm{o}} = 0.1$ and $\boldsymbol{u} = (0, 0)$, then two circular segments are formed outside sides S_1 and S_2 and also there is overlap between then. Hence, in this case, $F(\boldsymbol{u}; r_{\mathrm{o}}) = \pi r_{\mathrm{o}}^2 - (B_1(\boldsymbol{u}; r_{\mathrm{o}}) + B_2(\boldsymbol{u}; r_{\mathrm{o}}) - C_1(\boldsymbol{u}; r_{\mathrm{o}}))$. This will be further illustrated in the next section.

The *second challenge* is to average the CDF in (3) over the square. $F(\boldsymbol{u}; r_{\mathrm{o}})$ is a function of both the node location $\boldsymbol{u}$ and transmission range r_{o}. For a unit square, if $r_{\mathrm{o}} \geq \sqrt{2}$, then the disk $\mathcal{D}(\boldsymbol{u}; r_{\mathrm{o}})$ will cover the whole square $\mathcal{R}$ and hence $F(\boldsymbol{u}; r_{\mathrm{o}}) = 1$, irrespective of the node location. For intermediate values of the node range $0 \leq r_{\mathrm{o}} \leq \sqrt{2}$, both $\boldsymbol{u}$ and r_{o} need to be taken into account in determining $F(\boldsymbol{u}; r_{\mathrm{o}})$. This adds further complexity to the task of evaluating (4)$-$(6). A tractable exact solution to this problem is presented in the next section.

IV. PROPOSED FRAMEWORK

As illustrated in the last section, for a given value of the transmission range r_o and the location of the arbitrary node $\boldsymbol{u}$, $F(\boldsymbol{u}; r_\mathrm{o})$ can be expressed in closed-form using (7)−(10) and (11), (13)−(15). In order to facilitate the averaging of (3) over the whole square region, we consider different cases of the transmission range, as illustrated in Tables I and II. For each case of the range, the square region can be further subdivided into M subregions based on the different border and corner effects that occur in that region. Due to the symmetry of the square, some subregions have the same number of border and corner effects which can be exploited to further simplify the averaging.

Consider the *first case of the transmission range*, i.e., $0 \leq r_\mathrm{o} \leq \frac{1}{2}$, as shown in Fig. 2. This case may be of greatest interest in many practical situations where typically the sensor transmission range is a small fraction of the side length of the square. In this case, we can divide the square into four ($M = 4$) types of subregions $\mathcal{R}_1$, $\mathcal{R}_2$, $\mathcal{R}_3$ and $\mathcal{R}_4$, as shown in Fig. 2. It is easy to see that for an arbitrary node located anywhere in subregion $\mathcal{R}_1$, the disk $\mathcal{D}(\boldsymbol{u}; r_\mathrm{o})$ is completely inside the square $\mathcal{R}$, i.e., there are no border or corner effects. Hence, $F_1(\boldsymbol{u}; r_\mathrm{o}) = \pi r_\mathrm{o}^2$. For an arbitrary node located anywhere in subregion $\mathcal{R}_2$, the disk $\mathcal{D}(\boldsymbol{u}; r_\mathrm{o})$ is limited by side S_1, i.e., there is a circular segment formed outside the side S_1. Hence, $F_2(\boldsymbol{u}; r_\mathrm{o}) = \pi r_\mathrm{o}^2 - (B_1(\boldsymbol{u}; r_\mathrm{o}))$. For an arbitrary node located anywhere in subregion $\mathcal{R}_3$, the disk $\mathcal{D}(\boldsymbol{u}; r_\mathrm{o})$ is limited by sides S_1 and S_2, i.e., there is are two circular segments formed outside the sides S_1 and S_2 and there is no corner overlap between them. Hence, $F_3(\boldsymbol{u}; r_\mathrm{o}) = \pi r_\mathrm{o}^2 - (B_1(\boldsymbol{u}; r_\mathrm{o}) + B_2(\boldsymbol{u}; r_\mathrm{o}))$. For an arbitrary node located anywhere in subregion $\mathcal{R}_4$, the disk $\mathcal{D}(\boldsymbol{u}; r_\mathrm{o})$ is limited by sides S_1 and S_2 and vertex V_1, i.e., there is are two circular segments formed outside the sides S_1 and S_2 and there is corner overlap between them. Hence, $F_4(\boldsymbol{u}; r_\mathrm{o}) = \pi r_\mathrm{o}^2 - (B_1(\boldsymbol{u}; r_\mathrm{o}) + B_2(\boldsymbol{u}; r_\mathrm{o}) - C_1(\boldsymbol{u}; r_\mathrm{o}))$.

From Fig. 2, we can see that although there is one subregion of type $\mathcal{R}_1$, there are four subregions of types $\mathcal{R}_2$, $\mathcal{R}_3$ and $\mathcal{R}_4$, respectively, which are shaded in the same color for ease of identification, e.g., for an arbitrary node located in any subregion of type $\mathcal{R}_2$, the disk $\mathcal{D}(\boldsymbol{u}; r_\mathrm{o})$ is limited by one side only. Hence, we only need to average $F_i(\boldsymbol{u}; r_\mathrm{o})$ over one subregion of each type and multiply the result by the number of subregions of that type to ensure the entire square region is covered.

As r_o increases from 0 to $\frac{1}{2}$, we can see that the subregions of type $\mathcal{R}_1$ and $\mathcal{R}_2$ become smaller and the subregions of type $\mathcal{R}_3$ and $\mathcal{R}_4$ become larger. For the value of range $r_\mathrm{o} = \frac{1}{2}$, the subregions of type $\mathcal{R}_1$ and $\mathcal{R}_2$ approach zero. For the value of range $r_\mathrm{o} > \frac{1}{2}$, the subregions of type $\mathcal{R}_3$ and $\mathcal{R}_4$ overlap each other. While the subregions change with increasing value of the range, unique border and corner effects can be identified for each subregion. In total, 7 unique cases of the range can be identified as illustrated in Tables I and II. For each case of the range, the type $\mathcal{R}_i$, the number of subregions n_i and the corresponding closed form $F_i(\boldsymbol{u}; r_\mathrm{o})$ are tabulated in Tables I and II. Note that for the sake of brevity, $B_\ell(\boldsymbol{u}; r_\mathrm{o})$ and $C_\ell(\boldsymbol{u}; r_\mathrm{o})$ are written as B_ℓ and C_ℓ, respectively, for $\ell = 1, 2, 3, 4$ in Tables I and II.

Let $\mathcal{R}_1$, $\mathcal{R}_2$, $\ldots$ $\mathcal{R}_M$ denotes the type of subregions and n_i, $i \in \{1,\ 2\ \ldots,\ M\}$ denotes the number of subregion of type $\mathcal{R}_i$. Using (2) and (3), we can write the average probability of node isolation in (5) as

$$P_{\mathrm{iso}}(r_\mathrm{o}) = \sum_{i=1}^{M} n_i \int_{\mathcal{R}_i} \big(1 - F_i(\boldsymbol{u}; r_\mathrm{o})\big)^{N-1} ds(\boldsymbol{u}), \tag{19}$$

where $F_i(\boldsymbol{u}; r_\mathrm{o})$ denotes the probability that a random node falls inside the disk $\mathcal{D}(\boldsymbol{u}; r_\mathrm{o})$ of radius r_o centered at $\boldsymbol{u} \in \mathcal{R}_i$ and $\mathcal{R}_i$ and $F_i(\boldsymbol{u}; r_\mathrm{o})$ are defined in Tables I and II.

Remark 1: The division of the square $\mathcal{R}$ into subregions for transmission range $0 \leq r_\mathrm{o} \leq \frac{1}{2}$ has been previously shown in [12, Fig. 2] and [11, Fig. 7] to help illustrate the intuitive argument that the nodes situated in boundary subregions experience border effects. However, subregions $\mathcal{R}_3$ and $\mathcal{R}_4$ are indicated as one subregion in [11], [12]. Using our framework, we show that these are two distinct subregions with unique border and corner effects. In addition, we formulate all the subregions for all possible values of the transmission range.

Remark 2: The general formulation in (5) is also indirectly suggested in [11]. However, no guidelines are presented in order to evaluate (5). Hence, the authors in [11] use a deterministic grid deployment of nodes to approximate the boundary effects when nodes are uniformly and independently distributed in a square region. By contrast, we provide a tractable framework for complete and exact characterisation of boundary effects.

Remark 3: While $F_i(\boldsymbol{u}; r_\mathrm{o})$ in (3) can be expressed analytically in closed-form, the integration in (19) does not have a closed-form due to the $N-1$ factor in the exponent. However, it can be easily evaluated numerically using Tables I and II, which provide complete information for the exact evaluation of $P_{\text{iso}}(r_{\text{o}})$. It must be noted that numerical evaluation of two-fold integrals is widely practiced in the literature [19]. (19) will be used, along with Tables I and II, to calculate the probability of node isolation in finite wireless sensor networks formed in a square region.

Remark 4: We have considered a unit square region for the sake of simplicity in the proposed formulation. For the general case of a square of side length L, (19) can be used with appropriate scaling of the transmission range as $r_{\text{o}} \to r_{\text{o}}/L$.

V. NUMERICAL RESULTS

In this section, we present numerical results and compare with simulation results to validate the proposed framework. We also compare with results from prior work to demonstrate the advantage of our proposed framework, especially for smaller number of sensor nodes N. We have implemented (19) in Mathematica and the code is provided with this paper as supplementary material. We consider the nodes to be independently and uniformly distributed in a square region of side length $t = 1$. The simulation results are obtained by averaging over $10,000$ Monte Carlo simulation runs.

A. *Probability of Node Isolation*

Fig. 3 plots the probability of node isolation, $P_{\text{iso}}(r_{\text{o}})$, in (19) versus transmission range r_{o} for $N = 10, 25, 50, 100$ nodes. The probability of node isolation in infinite homogenous Poisson point process networks [3]

$$P_{\text{iso}}(r_{\text{o}}) = e^{-\rho\pi r_{\text{o}}^2}, \tag{20}$$

assuming constant node density $\rho = 10, 25, 50, 100$ nodes/m^2 is also plotted as a reference. We can see from Fig. 3 that the simulation results for finite networks match perfectly with the numerical results. This is to be expected since we account for boundary effects accurately and evaluate (19) exactly. Fig. 3 shows that the probability of node isolation is greater in finite networks, compared with Poisson networks. This is due to the inclusion of the border and corner effects, as explained in Section IV. Also the probability of node isolation decreases with increasing number of nodes, e.g., for finite networks the range required to achieve $P_{\text{iso}}(r_{\text{o}}) = 10^{-3}$ decreases from about $r_{\text{o}} = 0.65$ for $N = 10$ nodes to about $r_{\text{o}} = 0.18$ for $N = 100$ nodes.

B. Conditional Probability of Node Isolation

In order to illustrate the critical role played by the boundary effects in determining the probability of node isolation, we plot the conditional probability of node isolation $P_{\text{iso}}(\boldsymbol{u}; r_{\text{o}})$, in (4). Fig. 4 plots $P_{\text{iso}}(\boldsymbol{u}; r_{\text{o}})$ versus the position of an arbitrary node $\boldsymbol{u}(x, y)$ when $N = 10$ nodes, each with transmission range $r_{\text{o}} = 0.4$, which are uniformly and independently distributed in a unit square. We can see that the conditional probability of node isolation is minimum at the center of the square and maximum at the vertices. This is because the vertices experience the largest boundary effects. For $N = 10$ nodes and transmission range $r_{\text{o}} = 0.4$, the conditional probability of node isolation at any vertex is approximately 160 times higher than at the center. This shows that boundary effects are non-negligible in finite wireless sensor networks, especially when the number of nodes is small.

C. Probability of Connectivity

The probability of node isolation is closely coupled to the probability of connectivity. This is because we obtain a connected network at the same time as when we obtain a network with no isolated nodes, both with and without boundary effects [4], [5]. Fig. 5 plots the upper bound for the probability of connectivity, $P_{\text{con}}(r_{\text{o}})$, in (6) using (19), versus transmission range r_{o} for $N = 10, 100$ nodes. For comparison, we plot the high density approximation for $P_{\text{con}}(r_{\text{o}})$ which is derived in [13] using a cluster expansion approach as

$$P_{\text{con}}(r_{\text{o}}) \approx 1 - L^2 \rho e^{-\frac{\pi}{\beta}\rho} - 4L\sqrt{\frac{\beta}{\pi}} e^{-\frac{\pi}{2\beta}\rho} - \frac{16\beta}{\rho\pi} e^{-\frac{\pi}{4\beta}\rho}, \tag{21}$$

where L denotes the side length, ρ denotes the node density and $\beta = (r_{\text{o}}/L)^{-2}$. For reference, we also plot the $P_{\text{con}}(r_{\text{o}})$ for Poisson networks (without any boundary effects) [3]

$$P_{\text{con}}(r_{\text{o}}) = \left(1 - e^{-\rho\pi r_{\text{o}}^2}\right)^N . \tag{22}$$

It can be seen from Fig. 5 that the Poisson result (without boundary effects) is quite different from the finite network result, even for $N = 100$ nodes, which re-emphasises the importance of accurately characterising the boundary effects in finite wireless sensor networks. The high density approximation in (21) is quite accurate for $N = 100$ nodes but is not valid for $N = 10$ nodes. The upper bound for the probability of connectivity in (6) provides an excellent approximation for the simulation results when $P_{\text{con}}(r_{\text{o}})$ is larger than 0.95, irrespective of the number of nodes. This is consistent with the observation in [4] for circular areas with or without boundary effects. Thus, the proposed framework can be used to accurately predict the network connectivity properties even when the number of nodes is small.

D. *Conclusions*

In this paper, we have presented a tractable analytical framework for the exact calculation of probability of node isolation in finite wireless sensor networks. We have considered N sensor nodes, each with transmission range r_{o}, which are independently and uniformly distributed in a square region. The proposed framework can accurately account for the boundary effects by partitioning the square into subregions, based on the transmission range and the node location. The exact modelling of boundary effects has not been taken into consideration in previous studies in the literature. Our results confirm that boundary effects play a key role in determining the probability of node isolation and probability of connectivity, especially when the number of nodes is small $(N < 100)$. A summary of the key results in this paper is presented in Tables I and II.

REFERENCES

[1] G. Mao, "Research on wireless multi-hop networks: Current state and challenges," in *Proc. ICCNC*, 2012.

[2] F. Baccelli and B. Blaszczyszyn, *Stochastic geometry and wireless networks, volume 1 & 2: Theory and applications*. Foundations and Trends in Networking, 2009.

[3] C. Bettstetter, "On the minimum node degree and connectivity of a wireless multihop network," *Proc. 3rd ACM International Symposium on Mobile Ad Hoc Networking & Computing*, vol. 9, no. 11, pp. 80–91, 2002.

[4] ——, "On the connectivity of ad hoc networks," *The Computer Journal*, vol. 47, no. 4, pp. 432–447, 2004.

[5] M. Penrose, "The longest edge of the random minimal spanning tree," *The Annals of Applied Probability*, vol. 7, no. 2, pp. 340–361, 1997.

[6] P. Gupta and P. Kumar, "Critical power for asymptotic connectivity in wireless networks," in *Proc. IEEE CDC*, vol. 1, 1998, pp. 1106–1110.

[7] D. Miorandi, E. Altman, and G. Alfano, "The impact of channel randomness on coverage and connectivity of ad hoc and sensor networks," *IEEE Trans. Wireless Commun.*, vol. 7, no. 3, pp. 1062–1072, Mar. 2008.

[8] X. Zhou, S. Durrani, and H. M. Jones, "Connectivity analysis of wireless ad hoc networks with beamforming," *IEEE Trans. Veh. Technol.*, vol. 58, no. 9, pp. 5247–5257, Nov. 2009.

[9] W. Jia and J. Wang, "Analysis of connectivity for sensor networks using geometrical probability," *IEE Proceedings Communications*, vol. 153, no. 2, pp. 305–312, Apr. 2006.

[10] F. Fabbri and R. Verdone, "A statistical model for the connectivity of nodes in a multi-sink wireless sensor network over a bounded region," in *Proc. 14th European Wireless Conference*, June 2008.

[11] A. Eslami, M. Nekoui, H. Pishro-Nik, and F. Fekri, "Results on finite wireless sensor networks: Connectivity and coverage," *ArXiv Technical Report*, 2012. [Online]. Available: http://arxiv.org/abs/1211.2198

[12] G. Mao and B. D. O. Anderson, "Towards a better understanding of large-scale network models," *IEEE/ACM Transactions on Networking*, vol. 20, no. 2, pp. 408–421, Apr. 2012.

[13] J. P. Coon, C. P. Dettmann, and O. Georgiou, "Full connectivity: Corners, edges and faces," *J. Stat. Phys.*, vol. 147, pp. 758–778, 2012.

[14] J. G. Andrews, R. K. Ganti, M. Haenggi, N. Jindal, and S. Weber, "A primer on spatial modeling and analysis in wireless networks," *IEEE Commun. Mag.*, vol. 48, no. 11, pp. 156–163, Nov. 2010.

[15] P. Fan, G. Li, K. Cai, and K. Letaief, "On the geometrical characteristic of wireless ad-hoc networks and its application in network performance analysis," *IEEE Trans. Wireless Commun.*, vol. 6, no. 4, pp. 1256–1265, Apr. 2007.

[16] A. M. Mathai, *An introduction to geometrical probability: Distributional aspects with applications*. CRC Press, 1999.

[17] R. Rajagopalan and P. Varshney, "Connectivity analysis of wireless sensor networks with regular topologies in the presence of channel fading," *IEEE Trans. Wireless Commun.*, vol. 8, no. 7, pp. 3475–3483, Jul. 2009.

[18] Z. Khalid and S. Durrani, "Distance distributions in regular polygons," *ArXiv Technical Report*, 2012. [Online]. Available: http://arxiv.org/abs/1207.5857

[19] M. K. Simon and M.-S. Alouini, *Digital Communication over fading channels*, 2nd ed. Wiley, 2005.

LIST OF FIGURES

1 Illustration of border and corner effects in a unit square. 13

2 Subregions for the transmission range $0 \leq r_\mathrm{o} \leq \frac{1}{2}$ in a unit square. 14

3 Probability of node isolation, $P_\mathrm{iso}(r_\mathrm{o})$, versus transmission range r_o for $N = 10, 25, 50, 100$ nodes independently and uniformly distributed in a unit square. 15

4 Conditional probability of node isolation, $P_\mathrm{iso}(\boldsymbol{u}; r_\mathrm{o})$, versus position of arbitrary node $\boldsymbol{u}(x, y)$ for $N = 10$ nodes, each with transmission range $r_\mathrm{o} = 0.4$, which are independently and uniformly distributed in a unit square. 16

5 Probability of connectivity, $P_\mathrm{con}(r_\mathrm{o})$, versus transmission range r_o for $N = 10, 100$ nodes independently and uniformly distributed in a unit square. 17

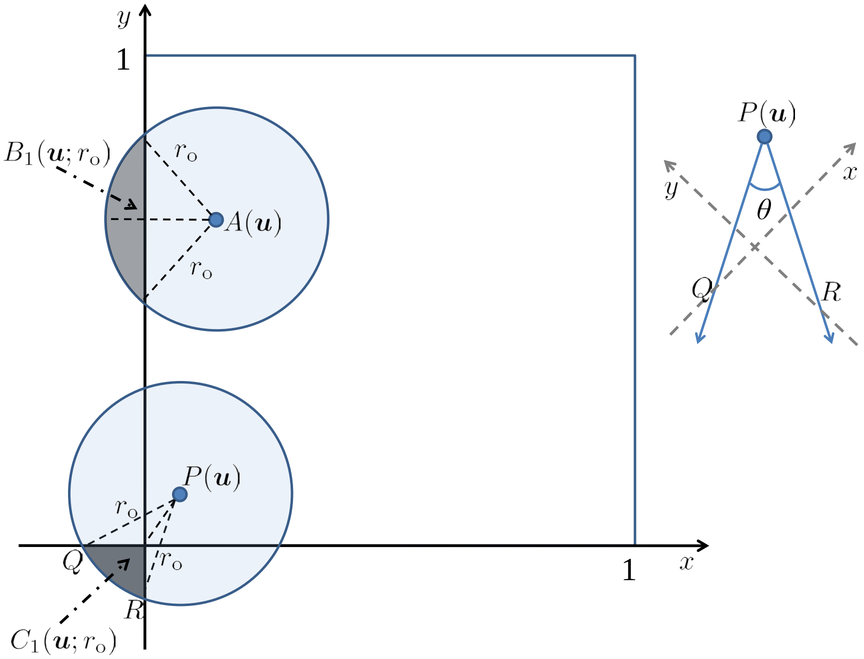

Fig. 1. Illustration of border and corner effects in a unit square.

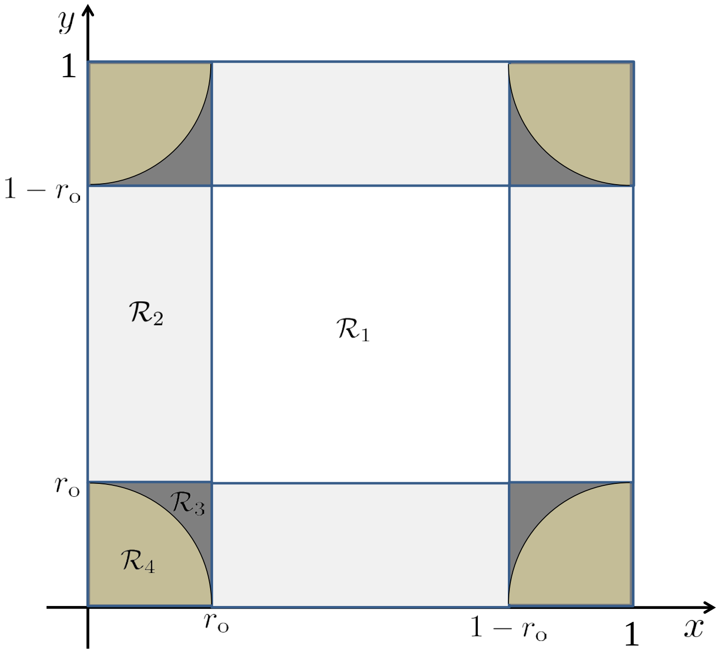

Fig. 2. Subregions for the transmission range $0 \leq r_{\rm o} \leq \frac{1}{2}$ in a unit square.

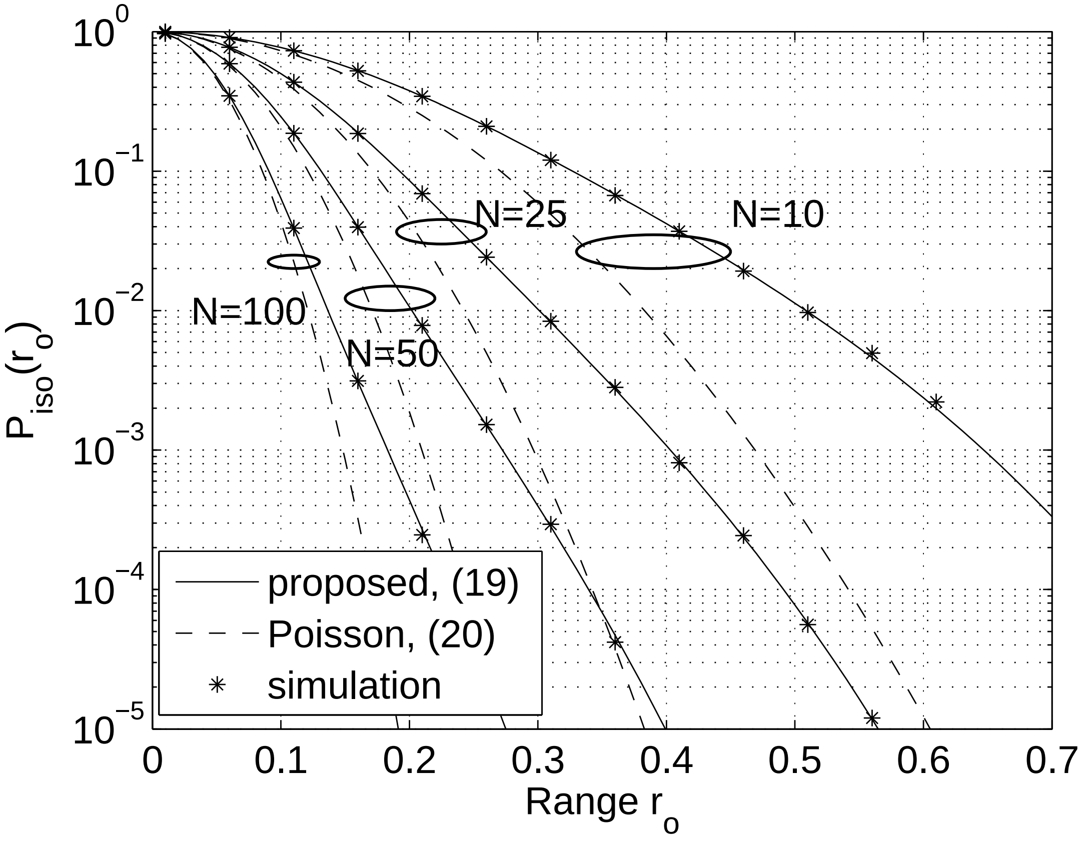

Fig. 3. Probability of node isolation, $P_{\rm iso}(r_{\rm o})$, versus transmission range $r_{\rm o}$ for $N = 10, 25, 50, 100$ nodes independently and uniformly distributed in a unit square.

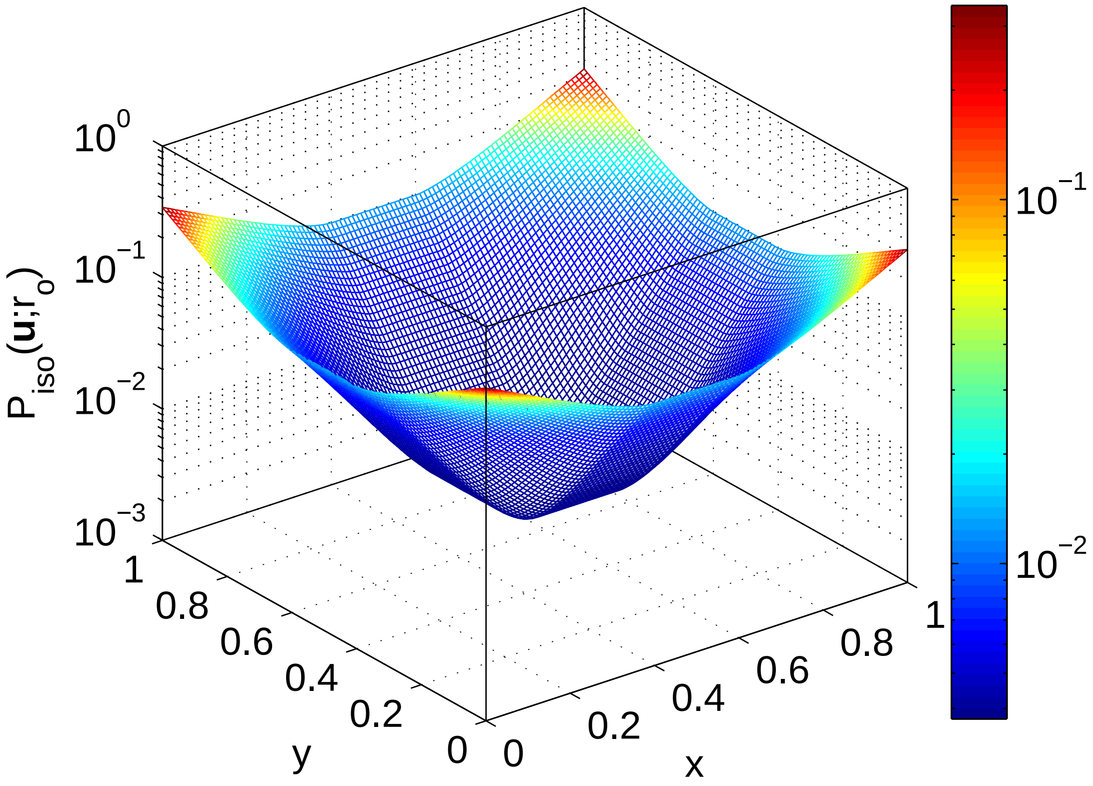

Fig. 4. Conditional probability of node isolation, $P_{\mathrm{iso}}(\boldsymbol{u}; r_{\mathrm{o}})$, versus position of arbitrary node $\boldsymbol{u}(x, y)$ for $N = 10$ nodes, each with transmission range $r_{\mathrm{o}} = 0.4$, which are independently and uniformly distributed in a unit square.

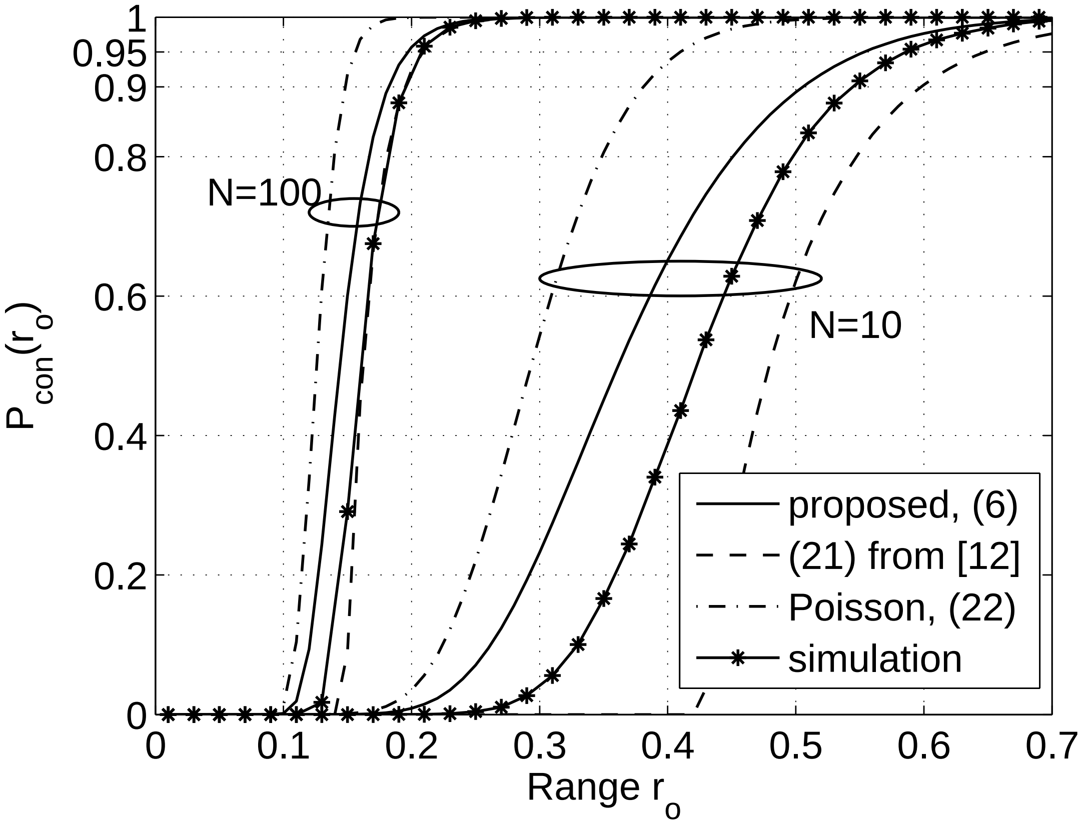

Fig. 5. Probability of connectivity, $P_{\text{con}}(r_{\text{o}})$, versus transmission range r_{o} for $N = 10, 100$ nodes independently and uniformly distributed in a unit square.

List of Tables

I Subregions and conditional probabilities for calculation of $P_{\mathrm{iso}}(r_{\mathrm{o}})$ $(0 < r_{\mathrm{o}} \leq \frac{1}{\sqrt{2}})$. 19
II Subregions and conditional probabilities for calculation of $P_{\mathrm{iso}}(r_{\mathrm{o}})$ $(\frac{1}{\sqrt{2}} < r_{\mathrm{o}} \leq \sqrt{2})$. 20

TABLE I

SUBREGIONS AND CONDITIONAL PROBABILITIES FOR CALCULATION OF $P_{\mathrm{iso}}(r_\mathrm{o})$ $(0 < r_\mathrm{o} \le \frac{1}{\sqrt{2}})$.

Range	Subregion $\mathcal{R}_i$	n_i	$F_i(\boldsymbol{u}; r_\mathrm{o})$
$0 \le r_\mathrm{o} \le \frac{1}{2}$	$\mathcal{R}_1 = \{x \in (r_\mathrm{o}, 1-r_\mathrm{o}),\, y \in (r_\mathrm{o}, 1-r_\mathrm{o})\}$	1	πr_o^2
	$\mathcal{R}_2 = \{x \in (0, r_\mathrm{o}),\, y \in (r_\mathrm{o}, 1-r_\mathrm{o})\}$	4	$\pi r_\mathrm{o}^2 - (B_1)$
	$\mathcal{R}_3 = \{x \in (0, r_\mathrm{o}),\, y \in (\sqrt{r_\mathrm{o}^2 - x^2}, 1)\}$	4	$\pi r_\mathrm{o}^2 - (B_1 + B_2)$
	$\mathcal{R}_4 = \{x \in (0, r_\mathrm{o}),\, y \in (0, \sqrt{r_\mathrm{o}^2 - x^2})\}$	4	$\pi r_\mathrm{o}^2 - (B_1 + B_2 - C_1)$
$\frac{1}{2} \le r_\mathrm{o} \le 2 - \sqrt{2}$	$\mathcal{R}_1 = \{x \in (0, \sqrt{2r_\mathrm{o} - 1}),\, y \in (0, 1-r_\mathrm{o})\} \cup \{x \in (\sqrt{2r_\mathrm{o} - 1}, 1-r_\mathrm{o}),\, y \in (0, \sqrt{r_\mathrm{o}^2 - x^2})\}$	4	$\pi r_\mathrm{o}^2 - (B_1 + B_2 - C_1)$
	$\mathcal{R}_2 = \{x \in (1-r_\mathrm{o}, 0.5),\, y \in (0, \sqrt{r_\mathrm{o}^2 - (x-1)^2})\}$	8	$\pi r_\mathrm{o}^2 - (B_1 + B_2 + B_3 - C_1 - C_2)$
	$\mathcal{R}_3 = \{x \in (1-r_\mathrm{o}, 0.5),\, y \in (\sqrt{r_\mathrm{o}^2 - (x-1)^2}, \sqrt{r_\mathrm{o}^2 - x^2})\}$	8	$\pi r_\mathrm{o}^2 - (B_1 + B_2 + B_3 - C_1)$
	$\mathcal{R}_4 = \{x \in (1-r_\mathrm{o}, 0.5),\, y \in (\sqrt{r_\mathrm{o}^2 - x^2}, 1-r_\mathrm{o})\}$	8	$\pi r_\mathrm{o}^2 - (B_1 + B_2 + B_3)$
	$\mathcal{R}_5 = \{x \in (\sqrt{2r_\mathrm{o} - 1}, 1-r_\mathrm{o}),\, y \in (\sqrt{r_\mathrm{o}^2 - x^2}, 1-r_\mathrm{o})\}$	4	$\pi r_\mathrm{o}^2 - (B_1 + B_2)$
	$\mathcal{R}_6 = \{x \in (1-r_\mathrm{o}, 0.5),\, y \in (1-r_\mathrm{o}, 0.5)\}$	4	$\pi r_\mathrm{o}^2 - (B_1 + B_2 + B_3 + B_4)$
$2 - \sqrt{2} \le r_\mathrm{o} \le \frac{5}{8}$	$\mathcal{R}_1 = \{x \in (0, 1-r_\mathrm{o}),\, y \in (0, 1-r_\mathrm{o})\}$	4	$\pi r_\mathrm{o}^2 - (B_1 + B_2 - C_1)$
	$\mathcal{R}_2 = \{x \in (1-r_\mathrm{o}, 0.5),\, y \in (0, \sqrt{r_\mathrm{o}^2 - (x-1)^2})\}$	8	$\pi r_\mathrm{o}^2 - (B_1 + B_2 + B_3 - C_1 - C_2)$
	$\mathcal{R}_3 = \{x \in (1-r_\mathrm{o}, \sqrt{2r_\mathrm{o} - 1}),\, y \in (\sqrt{r_\mathrm{o}^2 - (x-1)^2}, 1-r_\mathrm{o})\} \cup \{x \in (\sqrt{2r_\mathrm{o} - 1}, 0.5),\, y \in (\sqrt{r_\mathrm{o}^2 - (x-1)^2}, \sqrt{r_\mathrm{o}^2 - x^2})\}$	8	$\pi r_\mathrm{o}^2 - (B_1 + B_2 + B_3 - C_1)$
	$\mathcal{R}_4 = \{x \in (1-r_\mathrm{o}, \sqrt{2r_\mathrm{o} - 1}),\, y \in (1-r_\mathrm{o}, \sqrt{r_\mathrm{o}^2 - x^2})\}$	8	$\pi r_\mathrm{o}^2 - (B_1 + B_2 + B_3)$
	$\mathcal{R}_5 = \{x \in (\sqrt{2r_\mathrm{o} - 1}, 1-r_\mathrm{o}),\, y \in (\sqrt{r_\mathrm{o}^2 - x^2}, 1-r_\mathrm{o})\}$	4	$\pi r_\mathrm{o}^2 - (B_1 + B_2 + B_3 + B_4 - C_1)$
	$\mathcal{R}_6 = \{x \in (1-r_\mathrm{o}, \sqrt{2r_\mathrm{o} - 1}),\, y \in (\sqrt{r_\mathrm{o}^2 - x^2}, 0.5)\} \cup \{x \in (\sqrt{2r_\mathrm{o} - 1}, 0.5),\, y \in (1-r_\mathrm{o}, 0.5)\}$	4	$\pi r_\mathrm{o}^2 - (B_1 + B_2 + B_3 + B_4)$
$\frac{5}{8} \le r_\mathrm{o} \le \frac{1}{\sqrt{2}}$	$\mathcal{R}_1 = \{x \in (0, 1-r_\mathrm{o}),\, y \in (0, 1-r_\mathrm{o})\}$	4	$\pi r_\mathrm{o}^2 - (B_1 + B_2 - C_1)$
	$\mathcal{R}_2 = \{x \in (1-r_\mathrm{o}, 1-\sqrt{2r_\mathrm{o} - 1}),\, y \in (0, \sqrt{r_\mathrm{o}^2 - (x-1)^2})\} \cup \{x \in (1-\sqrt{2r_\mathrm{o} - 1}, 0.5),\, y \in (0, 1-r_\mathrm{o})\}$	8	$\pi r_\mathrm{o}^2 - (B_1 + B_2 + B_3 - C_1 - C_2)$
	$\mathcal{R}_3 = \{x \in (1-r_\mathrm{o}, 1-\sqrt{2r_\mathrm{o} - 1}),\, y \in (\sqrt{r_\mathrm{o}^2 - (x-1)^2}, 1-r_\mathrm{o})\}$	8	$\pi r_\mathrm{o}^2 - (B_1 + B_2 + B_3 - C_1)$
	$\mathcal{R}_4 = \{x \in (1-\sqrt{2r_\mathrm{o} - 1}, 0.5),\, y \in (1-r_\mathrm{o}, \sqrt{r_\mathrm{o}^2 - (x-1)^2})\}$	8	$\pi r_\mathrm{o}^2 - (B_1 + B_2 + B_3 + B_4 - C_1 - C_2)$
	$\mathcal{R}_5 = \{x \in (1-r_\mathrm{o}, \sqrt{r_\mathrm{o}^2 - 0.25}),\, y \in (1-r_\mathrm{o}, 1-\sqrt{r_\mathrm{o}^2 - x^2})\} \cup \{x \in (\sqrt{r_\mathrm{o}^2 - 0.25}, 1-\sqrt{2r_\mathrm{o} - 1}),\, y \in (1-r_\mathrm{o}, \sqrt{r_\mathrm{o}^2 - x^2})\} \cup \{x \in (1-\sqrt{2r_\mathrm{o} - 1}, 0.5),\, y \in (\sqrt{r_\mathrm{o}^2 - (x-1)^2}, \sqrt{r_\mathrm{o}^2 - x^2})\}$	4	$\pi r_\mathrm{o}^2 - (B_1 + B_2 + B_3 + B_4 - C_1)$
	$\mathcal{R}_6 = \{x \in (\sqrt{r_\mathrm{o}^2 - 0.25}, 0.5),\, y \in (\sqrt{r_\mathrm{o}^2 - x^2}, 0.5)\}$	4	$\pi r_\mathrm{o}^2 - (B_1 + B_2 + B_3 + B_4)$

TABLE II

SUBREGIONS AND CONDITIONAL PROBABILITIES FOR CALCULATION OF $P_{\mathrm{iso}}(r_{\mathrm{o}})$ ($\frac{1}{\sqrt{2}} < r_{\mathrm{o}} \leq \sqrt{2}$).

Range	Subregion $\mathcal{R}_i$	n_i	$F_i(\boldsymbol{u}; r_{\mathrm{o}})$
$\frac{1}{\sqrt{2}} \leq r_{\mathrm{o}} \leq 1$	$\mathcal{R}_1 = \{x \in (0, 1-r_{\mathrm{o}}),\ y \in (0, 1-r_{\mathrm{o}})\}$	4	$\pi r_{\mathrm{o}}^2 - (B_1 + B_2 - C_1)$
	$\mathcal{R}_2 = \{x \in (1-r_{\mathrm{o}}, 1-\sqrt{2r_{\mathrm{o}}-1}),\ y \in (0, \sqrt{r_{\mathrm{o}}^2-(x-1)^2})\} \cup \{x \in (1-\sqrt{2r_{\mathrm{o}}-1}, 0.5),\ y \in (0, 1-r_{\mathrm{o}})\}$	8	$\pi r_{\mathrm{o}}^2 - (B_1 + B_2 + B_3 - C_1 - C_2)$
	$\mathcal{R}_3 = \{x \in (1-r_{\mathrm{o}}, 1-\sqrt{2r_{\mathrm{o}}-1}),\ y \in (0, \sqrt{r_{\mathrm{o}}^2-(x-1)^2})\} \cup \{x \in (1-\sqrt{2r_{\mathrm{o}}-1}, 0.5),\ y \in (0, 1-r_{\mathrm{o}})\}$	8	$\pi r_{\mathrm{o}}^2 - (B_1 + B_2 + B_3 - C_1)$
	$\mathcal{R}_4 = \{x \in (1-\sqrt{2r_{\mathrm{o}}-1}, (1-\sqrt{2r_{\mathrm{o}}^2-1})/2),\ y \in (1-r_{\mathrm{o}}, \sqrt{r_{\mathrm{o}}^2-(x-1)^2})\} \cup \{x \in (1-\sqrt{2r_{\mathrm{o}}-1}, 0.5),\ y \in (1-r, 1-\sqrt{r_{\mathrm{o}}^2-x^2})\}$	8	$\pi r_{\mathrm{o}}^2 - (B_1 + B_2 + B_3 + B_4 - C_1 - C_2)$
	$\mathcal{R}_5 = \{x \in (1-r_{\mathrm{o}}, 1-\sqrt{2r_{\mathrm{o}}-1}),\ y \in (1-r_{\mathrm{o}}, 1-\sqrt{r_{\mathrm{o}}^2-x^2})\} \cup \{x \in (1-\sqrt{2r_{\mathrm{o}}-1}, (1-\sqrt{2r_{\mathrm{o}}^2-1})/2),\ y \in (\sqrt{r_{\mathrm{o}}^2-(x-1)^2}, 1-\sqrt{r_{\mathrm{o}}^2-x^2})\}$	4	$\pi r_{\mathrm{o}}^2 - (B_1 + B_2 + B_3 + B_4 - C_1)$
	$\mathcal{R}_6 = \{x \in ((1-\sqrt{2r_{\mathrm{o}}^2-1})/2, 1-\sqrt{r_{\mathrm{o}}^2-0.25}),\ y \in (1-\sqrt{r_{\mathrm{o}}^2-x^2}, \sqrt{r_{\mathrm{o}}^2-(x-1)^2})\} \cup \{x \in (1-\sqrt{r_{\mathrm{o}}^2-0.25}, 0.5), y \in (1-\sqrt{r_{\mathrm{o}}^2-x^2}, 1-\sqrt{r_{\mathrm{o}}^2-(x-1)^2})\}$	4	$\pi r_{\mathrm{o}}^2 - (B_1 + B_2 + B_3 + B_4 - C_1 - C_2 - C_4)$
	$\mathcal{R}_7 = \{x \in (1-\sqrt{r_{\mathrm{o}}^2-0.25}, 0.5),\ y \in (1-\sqrt{r_{\mathrm{o}}^2-(x-1)^2}, 0.5)\}$	4	$\pi r_{\mathrm{o}}^2 - (B_1 + B_2 + B_3 + B_4 - C_1 - C_2 - C_3 - C_4) = 1$
$1 \leq r_{\mathrm{o}} \leq \frac{\sqrt{5}}{2}$	$\mathcal{R}_1 = \{x \in (0, 1-\sqrt{r_{\mathrm{o}}^2-0.25}),\ y \in (0, \sqrt{r_{\mathrm{o}}^2-(x-1)^2})\} \cup \{x \in (1-\sqrt{r_{\mathrm{o}}^2-0.25}, \sqrt{r_{\mathrm{o}}^2-1}),\ y \in (0, 1-\sqrt{r_{\mathrm{o}}^2-(x-1)^2})\} \cup \{x \in (\sqrt{r_{\mathrm{o}}^2-1}, 0.5),\ y \in (1-\sqrt{r_{\mathrm{o}}^2-x^2}, 1-\sqrt{r_{\mathrm{o}}^2-(x-1)^2})\}$	4	$\pi r_{\mathrm{o}}^2 - (B_1 + B_2 + B_3 + B_4 - C_1 - C_2 - C_4)$
	$\mathcal{R}_2 = \{x \in (\sqrt{r_{\mathrm{o}}^2-1}, 0.5),\ y \in (0, 1-\sqrt{r_{\mathrm{o}}^2-x^2})\}$	8	$\pi r_{\mathrm{o}}^2 - (B_1 + B_2 + B_3 + B_4 - C_1 - C_2)$
	$\mathcal{R}_3 = \{x \in (1-\sqrt{r_{\mathrm{o}}^2-0.25}, 0.5),\ y \in (1-\sqrt{r_{\mathrm{o}}^2-(x-1)^2}, 0.5)\}$	4	$\pi r_{\mathrm{o}}^2 - (B_1 + B_2 + B_3 + B_4 - C_1 - C_2 - C_3 - C_4) = 1$
$\frac{\sqrt{5}}{2} \leq r_{\mathrm{o}} \leq \sqrt{2}$	$\mathcal{R}_1 = \{x \in (0, 1-\sqrt{r_{\mathrm{o}}^2-1}),\ y \in (0, 1-\sqrt{r_{\mathrm{o}}^2-(x-1)^2})\}$	4	$\pi r_{\mathrm{o}}^2 - (B_1 + B_2 + B_3 + B_4 - C_1 - C_2 - C_4)$
	$\mathcal{R}_2 = \{x \in (0, 1-\sqrt{r_{\mathrm{o}}^2-1}),\ y \in (1-\sqrt{r_{\mathrm{o}}^2-(x-1)^2}, 0.5)\} \cup \{x \in (1-\sqrt{r_{\mathrm{o}}^2-1}, 0.5),\ y \in (0, 0.5)\}$	4	$\pi r_{\mathrm{o}}^2 - (B_1 + B_2 + B_3 + B_4 - C_1 - C_2 - C_3 - C_4) = 1$